Published in final edited form as:

FEBS Lett. 2016 June ; 590(12): 1675–1686. doi:10.1002/1873-3468.12210.

Small Cargoes Pass Through Synthetically Glued Golgi Stacks

Julia Dancourt, **Hong Zheng**, **Francesca Bottanelli**, **Edward S. Allgeyer**, **Joerg Bewersdorf**, **Morven Graham**, **Xinran Liu**, **James E. Rothman**[$], and **Grégory Lavieu**[$]

Department of Cell Biology, Yale University, School of Medicine, New Haven, CT

Abstract

How are proteins transported across the stacked cisternae of the Golgi apparatus? Do they stay within the cisterna while the latter matures and progresses in an anterograde manner, or do they navigate between the cisternae via vesicles? Using synthetic biology, we engineered new tools designed to stabilize inter-cisternal adhesion such that Golgi cisternae are literally glued together, thus preventing any possible cisternal progression. Using bulk secretory assays and single cell live imaging, we observed that small cargoes (but not large aggregated cargoes including collagen) still transited through glued Golgi, although the rate of transport was moderately reduced. ARF1, whose membrane recruitment is required for budding COPI vesicles, continues to cycle on and off glued Golgi. Numerous COPI-size vesicles were intercalated among the glued Golgi cisternae. These results suggest that cisternal progression is not required for anterograde transport, but do not address the possibility of cisternal maturation in situ.

Introduction

The yeast *Saccharomyces cerevisiae* harbors well-separated Golgi cisternae and the early cis-Golgi cisterna is capable of maturing into a late trans-Golgi cisterna (1, 2). This suggests that anterograde cargoes are likely to follow the maturation path, without needing to leave the original cisterna. However in mammals the structure of the Golgi is much more complex and structured. Mammalian Golgi harbor multiple polarized, stacked cisternae that are laterally connected to form a ribbon structure (3). By homology with the yeast maturation mechanism, it has been proposed that cis-Golgi cisternae containing anterograde cargo mature and progress forward within the stack (4). The cisternal progression model has been supported by dynamic morphological studies (5), but the molecular machinery responsible for such a process has not yet been identified.

Another view considers Golgi cisternae as individual entities that are stable over a time that is at least compatible with several rounds of transport. In that case, COPI vesicles are thought to mediate cargo exchange between adjacent stacked-cisternae (6). The machinery responsible for such vesicular transport has been identified and extensively investigated both *in vitro* and *in vivo* (7). A morphological study (8) has also described the presence of anterograde cargo within these vesicles.

[$]Address correspondence to Grégory Lavieu gregory.lavieu@yale.edu and James. E Rothman james.rothman@yale.edu.

J.B. discloses significant financial interest in Bruker Corp.

In an effort to assess the predictions of each transport model, we have recently developed several synthetic biology approaches to alter the topology and stability of the Golgi stacks. Using a cell-cell fusion assay, we found that both anterograde and retrograde cargoes (i.e overexpressed Golgi-resident enzymes) can be carried by COPI vesicles, as long as the size of the cargo is compatible with their ~ 70 nm inner diameter (9). We used a drug-inducible system to “staple” and decorate Golgi cisternae in order to follow their fate. We observed that Golgi cisternae are composed of two domains: a static and inert central portion, and a rim that is the active transport zone required for both vesicular transport and transport of large aggregates like collagens by a novel process that we termed “rim progression”(10). Because large aggregate transport – but not small cargo transport – requires an intact ribbon (and does not take place effectively in individual “mini-stacks”) we suggested that anterograde transport of larger cargoes requires fission/fusion of the cisternal rims enclosing the aggregates among adjacent individual Golgi stacks within the ribbon (11), much as envisioned in the cisternal progenitor model (15)

On the other hand, Luini and colleagues used a very similar approach (i.e drug controlled-aggregation of a FM-aggregated Golgi-resident enzyme) to mark cisternae, and reached opposite conclusions (12). Their aggregated resident enzyme seemed to progress within the cisterna to the trans-Golgi face. Linstedt and colleagues (13) recently reported that FM-induced aggregation within the lumen of the Golgi can target the aggregated proteins for degradation in lysosomes, once they reach the trans-Golgi network. This suggests that aggregation within the Golgi lumen may ultimately result in a quality control response in many cases. It is noteworthy that the aggregates studied by Luini et al (12) were metabolically unstable during the several hours required to study transport, whereas the aggregates we employed were more stable.

With this in mind, we have now taken an orthogonal approach in which we artificially and stably glue adjacent Golgi cisternae together. This should permanently stabilize Golgi stacks and prevent any possible cisternal movements within them. We then explored the consequences of this new topology and constraint on the anterograde transport of small and large cargoes.

Results

A Golgi matrix-based glue

We engineered Golgi matrix proteins designed to interact exclusively at the cytosolic interface of the cis, medial, and trans Golgi cisternae (Figure 1A) in a drug-controlled manner (Figure 1A). We took advantage of the hetero-dimerization system that allows for FKBP/FRB interaction in the presence of the hetero-dimerizing drug (14), and can be used concomitantly with the FM-based aggregation/secretion system (15). We focused on matrix proteins grasp65 (G65), grasp55 (G55), and golgin97 (G97) that are well established to specifically decorate cis (16), medial (17) and trans-Golgi cisternae, respectively (18–20). G55 was fused to 3 FKBP repeats, whereas G65 and G97 were both fused to a single FRB domain (Figure 1A). Each chimeric protein was also tagged with a fluorescent protein to be appropriately visualized by light microscopy.

First we validated that the different components of the hypothetical glue (G65-FRB/G55-$FKBP_3$-CFP/RFP-FRB-G97) immuno-precipitated only in the presence of the hetero-dimerizing drug (Figure 1B). Secondly, we showed by confocal microscopy that cells expressing the glue components harbored an enlarged Golgi (identified by GT-YFP, a Golgi marker) in the presence of the hetero-dimerizing agent (Figure 1C and D). The structure of the ER was not obviously altered within cells harboring glued Golgi (Supplementary Figure 1D).

FRAP experiments revealed that the mobility within the Golgi area of G55-FKBP-CFP, which rapidly recovers (~10 second half-time) before dimerizer is added, was prolonged ~30 times by adding the dimerizing drug (Figure 1E upper graph and Supplementary Figure 1B upper panel). Similar results (~19 times slower recovery in the presence of the dimerizer) were observed when half-Golgi were photobleached (Figure 1E lower graph and Supplementary Figure 1B lower panel). This provides direct evidence that the components forming the inter-cisternal glue had indeed assembled with each other.

The glued-Golgi areas were always grossly enlarged as compared to untreated cells (visible at the light level; see Figure 1C). This alteration presented itself in various ways at the 2D-EM level. In some portions, the Golgi appeared as a giant flattened “hyper-stacked” ribbon closely opposed to rough ER (<10% of the cases); in other sections (>90% of the cases) it presented as an enlarged network of associated partly swollen Golgi cisternae (Supplementary Figure 1C). Because the later phenotype was more abundant we only further characterize by tomography the partly swollen cisternal presentation (Figure 3, Supplementary Figure 4A, B, and Supplementary Movie). This is discussed later. Note that electron dense structures were occasionally observed at the interface of the glued cisternae (Supplementary Movie and Supplementary Figure 4C), although this FKBP/FRB matrix-based glue was clearly not as electron dense as the much stronger FM_4-based aggregates (10, 21).

Immuno-EM confirmed that the assembled matrix-glue components were indeed highly concentrated (>4 fold increase) at the interfaces of opposed Golgi cisternae (Figure 1F and graph). As further evidence for successful gluing, the glued Golgi ribbons no longer dissociated into mini-stacks when microtubules were de-polymerized by nocodazole (Supplementary Figure 1A), suggesting that membrane fission is strongly inhibited within the core of the glued Golgi cisternae

Super-resolution microscopy revealed that cis and trans Golgi markers remained fully separated within the enlarged glued Golgi (Figure 1G). This suggests that the glued Golgi cisternae retained their proper identity. We note that the ribbon appeared thicker than in normal Golgi, consistent with our other results (Figure 1D and Supplementary Figure 1C).

Anterograde transport through glued Golgi

We recently proposed that transport of large cargoes via rim progression requires fusion/fission cycles between adjacent mini-stacks within the ribbon structure, whereas small cargoes utilize another secretory track(s) that do not require the ribbon organization (11). Gluing should prevent all forms of membrane mobility, including cisternae fission, and if so

is expected to block the proposed rim progression of large cargo. And, if small cargo can still transit static cisternae, it is predicted that small cargo but not large aggregated cargo should transit glued Golgi.

To test this, we measured the rate of secretion of small and large cargoes in populations of HeLa cells. The small cargoes (disaggregated FM-hGH and VSV-G) continued to be secreted, though at moderately reduced rates (1.8 and 1.4 fold decrease, respectively). By contrast, the large cargo (FM-hGH aggregated within the cis-Golgi) was strongly inhibited (5.5 fold decrease) (Figure 2A and Supplementary Figure 2). Confocal microcopy confirmed that Golgi-aggregated FM-hGH accumulated within the glued Golgi (Supplementary Figure 2B). Similar results were obtained with collagen-secreting fibroblasts (Saos-2 cells), in which we measured the rate of secretion of endogenous MMP2 (small cargo) and endogenous collagen-I aggregates (large cargo). The secretion of MMP2 was moderately inhibited (1.7 fold decrease), whereas the secretion of collagen aggregates was strongly (4.5 fold decrease) reduced (Figure 2A and Supplementary Figure 3A). Confocal microscopy confirmed that the retained collagen aggregates were located within the glued Golgi (Supplementary Figure 3B), suggesting that most of the transport inhibition occurs within the Golgi, and not earlier (i.e ER→Golgi).

Importantly, the inhibition of collagen aggregate transport was reversed when the glue was removed (Supplementary Figure 3C). Golgi enlargement phenotype was also reversed at the light microscopy level (data not shown). These results suggest that small cargoes are still transported within cells harboring glued Golgi, whereas large cargoes are largely retained, and therefore that the two types of cargoes follow different secretory pathways, consistent with our previous study (11).

We next extended the aforementioned population studies to single cells. Our strategy was to first select the cell to be monitored based on the size of the Golgi (expected to be enlarged when the Golgi is glued) and then to initiate a wave of cargo transport from the ER, using dynamic confocal imaging to monitor the appearance and disappearance of cargo from the Golgi over time. Then, at the end of the experiment, the cells were fixed and immuno-stained for collagen, to confirm its retention within the very same cell.

In control cells, fluorescently tagged small cargo completely filled the Golgi within 40 minutes, prior to being released progressively after an hour. As expected, at the end of the experiment, collagen was absent from the Golgi of these cells (Figure 2B left panel and lower graph). Transport of small cargoes still occurred in cells harboring glued Golgi, however the appearance of the cargo in the Golgi was delayed and now peaked at 90 minutes (Figure 2B right panel and lower graph). Cargo exit from the glued Golgi was sufficiently delayed that it was incomplete even at the end of the two-hour time course of live imaging. The retained portion of the cargo was located in the glued Golgi in these same single cells and co-localized with the blocked collagen (Figure 2B right panel). It is important to note that >85% of the cells that we had selected for live imaging based on the morphological criteria (enlarged Golgi) were later functionally validated as having retained collagen (Figure 2B upper graph). This validated that our judgment to select the cells to be imaged in real-time was appropriate. Furthermore, we may have imposed a selection bias towards

hyper-glued Golgi, which could explain why transport inhibition appeared stronger with single cell imaging than with the bulk secretion assay, which also include cells with poorly glued Golgi. The studies of single cells confirm and extend those from the population study.

To more sensitively investigate the effect of Golgi gluing on the kinetics of transport from to the cell surface we used TIRF microscopy. Consistent with the previous results, arrival of cargo at the cell surface still occurred within cells containing glued Golgi (Figure 2C), although the rate of transport was reduced. Importantly, in the absence of the disaggregating drug, no cargo reached the cell surface (Figure 2C, graph, black curve), ruling out any unspecific leak in our system.

The observed delay of transport could be due to a defect in ER→Golgi transport, intra-Golgi transport or Golgi→PM transport, or all of the above. To rule out a defect in Golgi→PM transport, we incubated the cell at 20°C for 4 hours to accumulate the released cargo in the TGN. We then measured the arrival at the PM by TIRF microscopy after releasing this temperature block (Figure 2D). The rate of TGN→PM transport was similar whether cells contained a glued Golgi or not, suggesting that the observed overall slowing of transport mainly occurs in the early secretory pathway and within the glued Golgi.

Mechanism of transport within glued Golgi

We used EM tomography to determine if COPI vesicles are found in the vicinity of the glued Golgi. First, we confirmed that most of the objects constituting the glued-Golgi network were cisternae (Figure 3A and Supplementary Movie). Most of these cisternae were so extended that they could not be entirely captured within the 250 nm thickness of the electron-tomographic sample. We found that vesicles (50–100 nm spherical objects entirely resolved within the 250 nm) were found within the glued Golgi at an average density of $60/\mu m^3$ (Figure 3A). These vesicles were not homogeneously distributed but seemed to concentrate in “hot-spots”, where they were intercalated within the maze of the glued Golgi cisternae (Figure 3B). This is consistent with these being intra-Golgi vesicles responsible for the transport activity. We therefore tested the dynamics of ARF1-GFP, a required component of COPI vesicles, by FRAP of glued Golgi membranes. ARF1-GFP turnover on Golgi membrane was very similar whether the Golgi was glued or not (recovery half-times of 13 and 14 sec, respectively) (Figure 3C). However, the mobile fraction of ARF1-GFP was slightly reduced within glued Golgi (1.3 fold decrease) consistent with the slowdown of transport reported earlier. This suggested that the machinery responsible for vesicle budding within the Golgi is functional, even in glued Golgi. Therefore, we concluded that vesicles might be responsible for the remaining anterograde transport activity observed in cells harboring glued Golgi. These vesicles may also be involved in the recycling of Golgi resident proteins.

Discussion

We engineered tools that literally glue Golgi cisternae together over a prolonged period (> 15 hours) during which about 50 complete cycles of import and export of cargo would normally occur (assuming about 20 min Golgi transit time). Yet, despite this, anterograde transport of secretory and membrane proteins continue largely unimpeded. It is hard to

reconcile this dramatic finding with models in which cisternae must move progressively from one end of the stack to the other to carry such cargo. Gluing should prevent the trans-most cisterna from leaving in this model, but should not prevent addition of new membrane (from ER) at the cis face to form new cisternae, so the number of cisternae should increase and membranes should massively accumulate at the cis pole of the stack. This was not observed.

Furthermore, protein aggregates are retained within the glued Golgi, implying that even if cisternal progression had been taking place before gluing (as the mechanism of aggregate transport) it must have been stopped by gluing. This underscores that the ongoing transport of small cargo after gluing could not result from cisternal progression.

It is especially important for the interpretation of our results to explicitly distinguish between the concepts of cisternal maturation (a given cisterna takes on the composition of a later cisterna over time) and cisternal progression (a given cisterna physically moves up in the stack), our results speak strongly against progression as being responsible for the majority of anterograde transport but do not address the possibility that maturation could continue within the glued Golgi stacks. Thus, recycling COPI vesicles could be formed at the edges of the glued cisternae, and formation of secretory vesicles could still occur within a static cis-glued cisterna that is reaching a TGN-like state. This could satisfyingly explain the transport of small cargo. But why large cargo transport would be more dramatically affected then?

The Golgi stack is, by definition, perturbed by gluing, and the transport of small anterograde cargo is slower than before gluing. But to minimize the degree of perturbation, we chose a glue based on the very matrix proteins that are naturally positioned at the interface of Golgi cisternae, where they normally contribute to establish inter-cisternal adhesion. We merely used synthetic approaches to strengthen these interactions and render them permanent. In addition, the location of this perturbation to the cytoplasmic side of the cisternae avoids the theoretical possibility of contact/interference with lumenal cargo. In light of this and the considerations above, our experiments cannot address whether cisternal progression is responsible for the fraction of anterograde transport corresponding to reduction in rate after gluing; rather, we can only conclude that cisternal progression is not the only mechanism capable of anterograde transport.

The simplest explanation is that the small cargoes move through COPI vesicles, which are known to bud at the rims of cisternae at all levels of the stack (8). Indeed, we readily observed these vesicles within the vicinity of the glued Golgi. In fact the density of COPI-size vesicles in glued Golgi areas (~ 60 vesicles/μm^3) is slightly lower to that reported for unperturbed Golgi areas (~ 100 vesicles/μm^3; (22)), consistently with the reported transport slow down.

In the long run it will be vital to observe and quantify the patterns of protein traffic in the Golgi directly using dynamic, molecularly specific imaging at super-resolution. Until that technology emerges, the field will need to rely on indirect methods involving one or another kind of perturbation, and the strength of conclusions needs to be calibrated with this in mind.

The more orthogonal methods that are applied the better. Neither trans-lumenal stapling of cisterna (10) nor permanently gluing them together grossly impede anterograde transport; in both conditions the cisternae were shown to be (10) or rendered (this study) immobile.

Materials and Methods

Cell culture and transfection

HeLa and Saos-2 cells were maintained in DMEM medium (Gibco, Grand Island, NY, U.S.A.) supplemented with 10 % fetal bovine serum (Sigma-Aldrich, St Louis, MO, U.S.A.) at 37°C under 5% CO_2. 25 μg/mL ascorbate (Sigma-Aldrich) was further added to Saos-2 cells medium. Hela cells were transfected using Lipofectamine 2000 (Invitrogen, Grand Island, NY, U.S.A.) according to the manufacturer's instructions. Saos-2 cells were electroporated using the Nepa21 electroporator (Nepagene, Chiba, Japan).

Plasmids, antibodies and reagents

ss-GFP-FM4-hGH was described previously (21). VSV-G^{ts}-GFP was ordered from Addgene (Cambridge, MA, United States). DsRed-FRB-Golgin97 (DsRed-FRB-G97), GRASP55-FKBP3-CFP (G55-$FKBP_3$-CFP), GRASP55-FKBP, GRASP65-FRB-YFP (G65-FRB-YFP) and GRASP65-FRB were generated by sequential insertion of CFP (or YFP, or DsRed), and the indicated Golgi protein-encoding sequences into a pC4-ss-FM backbone vector (ARIAD), using XbaI/SpeI compatibility and the BamH1 restriction site. GRASP65-, GRASP55- and Golgin97-encoding plasmids were a gift from Y. Wang, A. Linstedt and S. Munro, respectively. GT-YFP and ARF1-GFP plasmids were kind gifts from C. Giraudo and G. Romero respectively.

For immunoblotting and immunofluorescence microscopy, antibodies used were anti-mCherry (Biovision, Milpitas, CA, U.S.A.), anti-Collagen-I (Developmental Studies Hybridoma Bank, Iowa City, IA, U.S.A.), anti-MMP2 (Cell Signaling, Boston, MA, U.S.A.), anti-GFP (Roche, Brandford, CT, U.S.A.), anti-HA (Covance, Princeton, NJ, U.S.A.), anti-VSV-G P5D4 (12). anti-Grasp65 (Sigma-Aldrich), and anti-hGH (Dako, Carpinteria, CA, U.S.A.). The anti-Grp78 antibody was a kind gift from T. Walter. The $Atto^{647}$-conjugated secondary antibody we used was from Sigma-Aldrich.

A/C heterodimerizer and D/D solubilizer were from Clontech Laboratories (Mountain View, CA, U.S.A.) and used at 1 μM for the indicated amount of time. Nocodazole (Sigma-Aldrich) was used at 1 μg/mL for 2 hours.

Electron microscopy

For regular epon embedding, cells were fixed in 2.5% gluteraldehyde in 0.1 M sodium cacodylate buffer pH7.4 before being scraped and pelleted in 2% agar, then post-fixed in 1% osmium tetroxide and en bloc stained in 2% uranyl acetate. Samples were then dehydrated in an ethanol series and infiltrated with resin (Electron Microscopy Science, Hatfield, PA, U.S.A.). Hardened blocks were cut using a Leica UltraCut UC7 (Buffalo Grove, IL, U.S.A.), 60 nm sections were collected and stained using 2% uranyl acetate and lead citrate.

For immuno-electron microscopy using LR White (London Resin White), samples were fixed in 4% paraformaldehyde/0.1% gluteraldehyde in PBS before being rinsed in PBS and blocked with 50 mM NH4Cl +100mM glycine. Cells were then scraped in 1% gelatin, and transferred to 2% Agar on ice. Samples were trimmed and rinsed in Tris 50 mM Maleate + 3.5% sucrose twice and placed in 2% uranyl acetate/Tris + 50 mM Maleate. After rinsing again they were dehydrated in an ethanol series, then infiltrated with 50:50 ethanol/LR White (Electron Microscopy Science), followed by several changes of pure 100% LR White. Samples were polymerized and sections were collected on carbon/ formvar coated nickel grids. Grids were placed section side down on drops of 0.1M ammonium chloride to quench untreated aldehyde groups, then blocked for nonspecific binding on 1% fish skin gelatin in PBS. Grids were then incubated with the polyclonal anti-DsRed primary antibody (1:200; Clontech Laboratories), rinsed in PBS followed by incubation with 10 nm Protein A gold (Utrecht Medical Center). Grids were rinsed in PBS, post-fixed using 1% gluteraldehyde, contrast stained using aqueous uranyl acetate and lead citrate.

Samples were all viewed on FEI Tencai Biotwin TEM at 80Kv. Images were taken using Morada CCD and iTEM (Olympus, Waltham, MA, U.S.A.) software.

Electron tomography on 250nm sections was done using FEI Tecnai TF20 at 200 Kv tilting from 60 to –60 degrees. Data was collected using FEI Eagle 1×1 and reconstructed and modeled using IMOD (University of Colorado, Boulder, CO, U.S.A.).

For surface density calculations, the number of gold particles associated with a structure was counted, and the membrane length was measured using ImageJ. The density was then expressed as LD (number of gold particles/micrometer).

Fluorescence microscopy

For immunofluorescence, cells were grown on glass coverslips in 24-well plates and were fixed with 4% paraformaldehyde before being triton permeabilized and incubated with the appropriate antibodies. For live cell imaging, Saos-2 cells were grown in glass bottom dishes (MatTek, Ashland, MA, U.S.A.) and imaged in Live Cell Imaging Solution (Invitrogen) supplemented with 10 mM Glucose and 25 μg/mL ascorbate (Sigma-Aldrich). For cargo release, cells were incubated with 100 μg/mL cycloheximide (Sigma-Aldrich) and D/D solubilizer for the indicated amount of time. Live cell imaging was performed at 37°C. Images were obtained on a Zeiss LSM510 microscope.

For FRAP experiments we used a multicolor spinning-disk confocal based on an inverted Olympus microscope (IX-71) and Perkin-Elmer Ultraview system with 5-laser and FRAP/photoactivation. GRASP55-FKBP3-CFP or ARF1-GFP were photobleached within the Golgi region at 440 nm (90% laser power) for 0.5 seconds and 488 nm (20% laser power) for 2 seconds respectively. Stimulated emission depletion microscopy was performed on a custom system built around an inverted microscope base (IX-71, Olympus, Japan). A depletion wavelength of 775 nm is employed from an 80 MHz repetition rate, 650 ps pulsed, laser (Katana HP, One Five, Switzerland) which is coupled into a polarization maintaining (PM) single-mode fiber. The collimated fiber output is directed onto a spatial light modulator (X10468-02, Hamamatsu, Japan) for aberration control and application of a

helical phase ramp to create a ring shaped depletion focus. The SLM is imaged onto a 16 kHz resonant mirror (SC-30, Electro-Optical Products Corp., U.S.A) which is, in turn, imaged on to the back pupil plane of a 100× oil immersion objective lens (UPLSAPO 100× Oil PSF, Olympus, Japan). Fluorescence excitation is provided by two pulsed diode lasers emitting laser pulses of approximately 80 ps at wavelengths of 650 nm and 595 nm (LDH-D-C-650 and LDH-TA-595, PicoQuant GmbH, Germany), which are electronically synchronized to the depletion laser via custom built electronics (Opsero Electronic Design, Canada). The excitation beams are combined with the depletion beam via a dichroic mirror (zt750spxr, Chroma) after passing through a PM single-mode fiber. Scanning the overlaid depletion and excitation foci through the focal plane is accomplished with the aforementioned 16 kHz resonant mirror for the fast axis and a synchronized galvanometer pair for the slow axis. Fluorescence is collected by the same objective, de-scanned, and separated from back scattered excitation and depletion light with a custom dichroic mirror (zt485/595/640/775rpc, Chroma). Fluorescence from STAR635P and ATTO594 is then split with a dichroic mirror (zt640rdc, Chroma) and directed through respective band pass filters (FF02-685/40-25 and FF01-624/40-25, Semrock), focused into 125 μm core multimode fibers acting as confocal pinholes (approximately 0.8 Airy units), and collected via single-photon counting avalanche photodiodes (APD) (SPCM-ARQ-13-FC, Excelitas, Canada). APD outputs are connected to custom electronics (Opsero Electronic Design, Canada) that gate the detection signal relative to the excitation laser pulses before being passed to a field programmable gate array board (PCIe-7852R, National Instruments, U.S.A) that organizes photon counts into lines of the image before passing them to the host computer. System control is realized using a custom interface (LabVIEW, National Instruments, U.S.A) with the ability to collect images sequentially or simultaneous in a line-by-line mode.

For TIRF microscopy, Saos-2 cells were handled as for live cell confocal microscopy. Immunofluorescence for STED imaging was performed using an anti-TGN46 antibody generated in sheep (Ab serotec) and an anti-GM130 antibody generated in mouse (BD biosciences laboratories). As secondary antibodies anti-mouse STAR635P antibodies (Abberior) and anti-Sheep ATTO594 generated in the lab were used. Conjugation of unlabelled anti-Sheep IgGs (Jackson Immunoresearch) was performed in a 10% 1M Sodium bicarbonate with a molar ratio of ATTO590 NHS ester (SIGMA):antibodies of 50:1. The reaction was incubated at room temperature for 1 hour and the excess free dye was separated using a Micro Bio-Spin column MWCO=6KDa (BIORAD).

Co-immunoprecipitation

Cells were grown in 6-well plate and transfected with the appropriate combination of plasmids. When required, the dimerizing drug was added overnight and maintained during the procedure. Cells were collected and resuspended in lysis buffer (1% Triton X-100, 5mM EDTA, 150mM NaCl pH 7.4 and 1% protease inhibitor). The cell lysate was centrifuged, and the supernatant was collected and incubated with anti-GFP antibody (Roche, Penzberg, Germany) and Protein-A agarose beads (Roche, Penzberg, Germany) for 2 hours at 4°C. After centrifugation, protein-A interacting proteins were eluted from the beads with SDS-sample buffer. Samples were then analyzed by SDS-PAGE and immunoblotting.

Secretion assays

Cell surface biotinylation, TCA precipitation, SDS-PAGE and immunoblot analysis were performed as described previously (10).

Image analysis and statistics

All graphs were rendered in GraphPad Prism (La Jolla, CA, U.S.A.) as averaged data ± standard error of the mean (s.e.m.).

FRAP was quantified using Volocity (PerkinElmer, Walthham, MA, U.S.A.) and single corrected (background corrected).

Densitometry for immunoblots, as well as fluorescence intensity and area size on micrographs were quantified using ImageJ. Fluorescence intensity for live imaging was background corrected and expressed as fold increase.

Supplementary Material

Refer to Web version on PubMed Central for supplementary material.

Acknowledgments

We thank Derek Toomre and Felix Rivera-Molina for assistance with the TIRF microscopy. We thank Myun Hwa Dunlop for kindly reading and editing the manuscript. This work was supported by the NIH (R01 GM 095532). J.B was supported by Wellcome Trust (095927/A/11/Z).

Abbreviation List

ARF1	ADP-ribosylation factor 1
COPI	**co**at **p**rotein complex I
FRAP	Fluorescence Recovery After Photobleaching
GFP	Green Fluorescent Protein
RFP	Red Fluorescence Protein
EM	Electron Microscopy
ER	Endoplasmic Reticulum
PM	Plasma Membrane
CHX	Cycloheximide
VSV-G	Vesicular Stomatitis Virus glycoprotein
TGN	Trans Golgi Network
GRASP	Golgi Re-Assembly Stacking Protein
MMP2	matrix metalloproteinase-2

GT Galactosyl-Transferase

References

1. Losev E, et al. Golgi maturation visualized in living yeast. Nature. 2006 Jun 22.441:1002. [PubMed: 16699524]
2. Matsuura-Tokita K, Takeuchi M, Ichihara A, Mikuriya K, Nakano A. Live imaging of yeast Golgi cisternal maturation. Nature. 2006 Jun 22.441:1007. [PubMed: 16699523]
3. Klumperman J. Architecture of the mammalian Golgi. Cold Spring Harbor perspectives in biology. 2011 Jul.3
4. Beams HV, Kessel RG. The Golgi apparatus: structure and function. Int. Rev. Cytol. 1968; 23:209. [PubMed: 4873473]
5. Bonfanti L, et al. Procollagen traverses the Golgi stack without leaving the lumen of cisternae: evidence for cisternal maturation. Cell. 1998 Dec 23.95:993. [PubMed: 9875853]
6. Pelham HR, Rothman JE. The debate about transport in the Golgi--two sides of the same coin? Cell. 2000 Sep 15.102:713. [PubMed: 11030615]
7. Rothman JE. The principle of membrane fusion in the cell (Nobel lecture). Angew Chem Int Ed Engl. 2014 Nov 17.53:12676. [PubMed: 25087728]
8. Orci L, et al. Bidirectional transport by distinct populations of COPI-coated vesicles. Cell. 1997 Jul 25.90:335. [PubMed: 9244307]
9. Pellett PA, Dietrich F, Bewersdorf J, Rothman JE, Lavieu G. Inter-Golgi transport mediated by COPI-containing vesicles carrying small cargoes. eLife. 2013; 2:e01296. [PubMed: 24137546]
10. Lavieu G, Zheng H, Rothman JE. Stapled Golgi cisternae remain in place as cargo passes through the stack. eLife. 2013; 2:e00558. [PubMed: 23755362]
11. Lavieu G, et al. The Golgi ribbon structure facilitates anterograde transport of large cargoes. Molecular biology of the cell. 2014 Oct 1.25:3028. [PubMed: 25103235]
12. Rizzo R, et al. The dynamics of engineered resident proteins in the mammalian Golgi complex relies on cisternal maturation. The Journal of cell biology. 2013 Jun 24.201:1027. [PubMed: 23775191]
13. Tewari R, Bachert C, Linstedt AD. Induced oligomerization targets Golgi proteins for degradation in lysosomes. Molecular biology of the cell. 2015 Dec 1.26:4427. [PubMed: 26446839]
14. Lavieu G, et al. Induction of cortical endoplasmic reticulum by dimerization of a coatomer-binding peptide anchored to endoplasmic reticulum membranes. Proceedings of the National Academy of Sciences of the United States of America. 2010 Apr 13.107:6876. [PubMed: 20351264]
15. Rivera VM, et al. Regulation of protein secretion through controlled aggregation in the endoplasmic reticulum. Science. 2000 Feb 4.287:826. [PubMed: 10657290]
16. Barr FA, Puype M, Vandekerckhove J, Warren G. GRASP65, a protein involved in the stacking of Golgi cisternae. Cell. 1997 Oct 17.91:253. [PubMed: 9346242]
17. Shorter J, et al. GRASP55, a second mammalian GRASP protein involved in the stacking of Golgi cisternae in a cell-free system. The EMBO journal. 1999 Sep 15.18:4949. [PubMed: 10487747]
18. Barr FA. A novel Rab6-interacting domain defines a family of Golgi-targeted coiled-coil proteins. Current biology : CB. 1999 Apr 8.9:381. [PubMed: 10209123]
19. Kjer-Nielsen L, Teasdale RD, van Vliet C, Gleeson PA. A novel Golgi-localisation domain shared by a class of coiled-coil peripheral membrane proteins. Current biology : CB. 1999 Apr 8.9:385. [PubMed: 10209125]
20. Munro S, Nichols BJ. The GRIP domain - a novel Golgi-targeting domain found in several coiled-coil proteins. Current biology : CB. 1999 Apr 8.9:377. [PubMed: 10209120]
21. Volchuk A, et al. Megavesicles implicated in the rapid transport of intracisternal aggregates across the Golgi stack. Cell. 2000 Aug 4.102:335. [PubMed: 10975524]
22. Ladinsky MS, Mastronarde DN, McIntosh JR, Howell KE, Staehelin LA. Golgi structure in three dimensions: functional insights from the normal rat kidney cell. The Journal of cell biology. 1999 Mar 22.144:1135. [PubMed: 10087259]

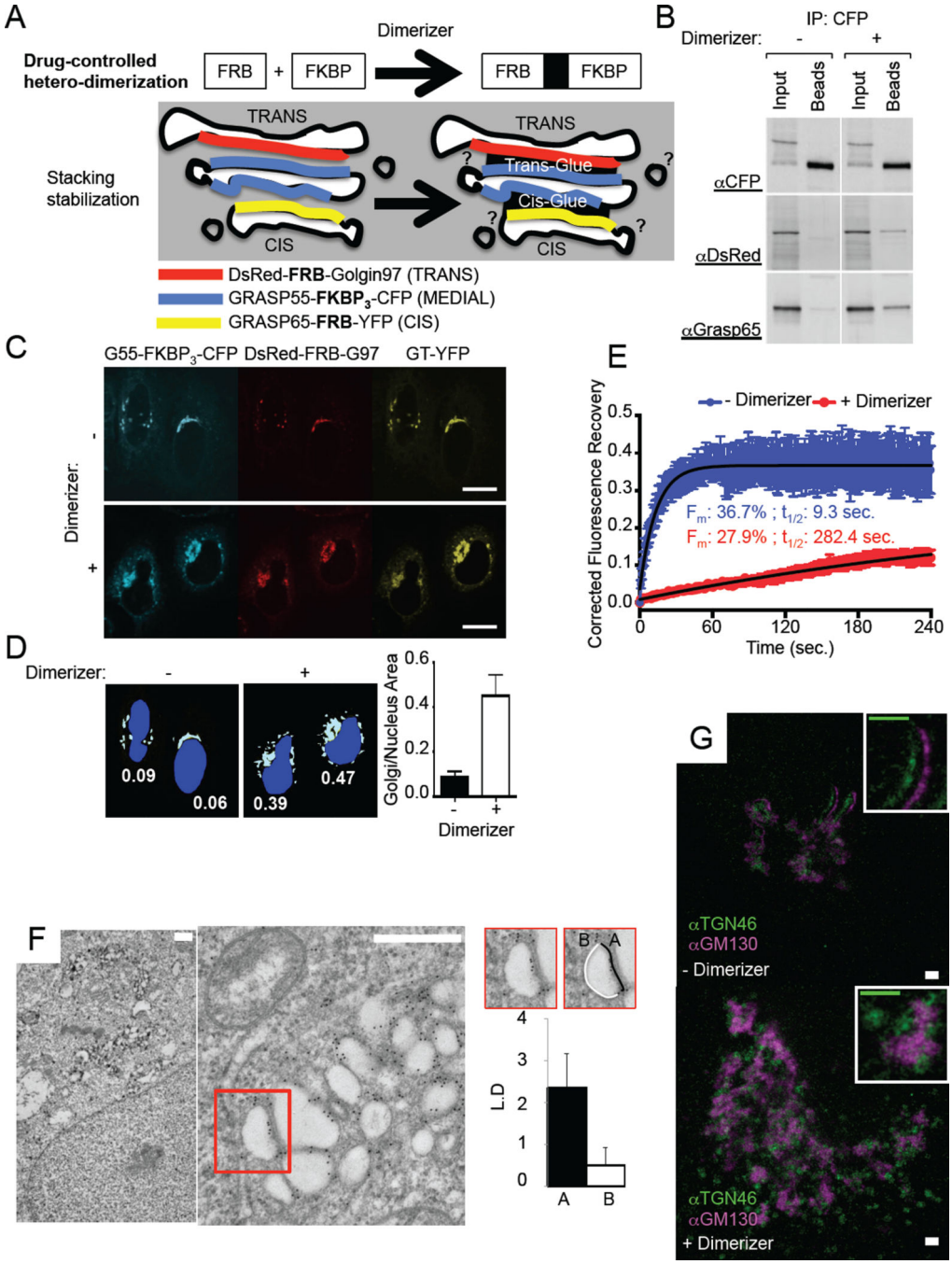

Figure 1. Gluing Golgi cisternae to stabilize the ribbon

A. Cartoon depicting the approach used to form a glued Golgi. Golgin97 (G97), Grasp55 (G55) and Grasp65 (G65) are fused to protein domains allowing their drug-controlled hetero-dimerization as well as to fluorescent proteins for visualization purposes. Upon Dimerizer treatment, the different constructs come together to glue cis and trans faces of the Golgi stack. B. Lysates from HeLa cells expressing DsRed-FRB-Golgin97, Grasp55-$FKBP_3$-CFP and Grasp65-FRB, treated or not with Dimerizer for 16 hours, were subjected to anti-CFP co-immunoprecipitation. Immunoprecipitates were resolved by SDS-PAGE and

visualized by western blot using anti-CFP, anti-DsRed or anti-Grasp65 antibodies to detect the three different constructs expressed. C. HeLa cells expressing DsRed-FRB-Golgin97, Grasp55-$FKBP_3$-CFP, Grasp65-FRB and GT-YFP, treated or not with Dimerizer for 16 hours, were visualized by confocal microscopy. The areas delineating the nucleus and the Golgi (labeled with GT-YFP) were measured and ratioed for 18 cells for each condition as plotted in D. Scale bars: 10 μm. E. Fluorescence Recovery After Photobleaching experiments were performed on HeLa cells expressing DsRed-FRB-Golgin97, Grasp55-$FKBP_3$-CFP and Grasp65-FRB with (green) or without (blue) Dimerizer. CFP fluorescence was bleached and its recovery monitored within full or Half Golgi region (see Fig. S1B). Data was single-corrected and averaged over at least 9 cells taken from two independent experiments. Data was fitted on a one-phase association curve (red line). F. HeLa cells expressing DsRed-FRB-Golgin97, Grasp55-$FKBP_3$-CFP and Grasp65-FRB-YFP and treated with Dimerizer, were processed for immuno-electron microscopy against DsRed. Scale bars: 500nm. Graph, Gold particle concentration (Linear Density) at membrane facing opposed Golgi membrane (A) or cytosol (B). Quantification was performed on >20 Golgi. G. HeLa cells expressing GFP-FRB-Golgin97, Grasp55-$FKBP_3$-CFP and Grasp65-FRB, treated or not with Dimerizer for 16 hours, were immunolabeled with anti-TGN46 and anti-GM130 antibodies and observed by STED microscopy. Scale bars: 1 μm.

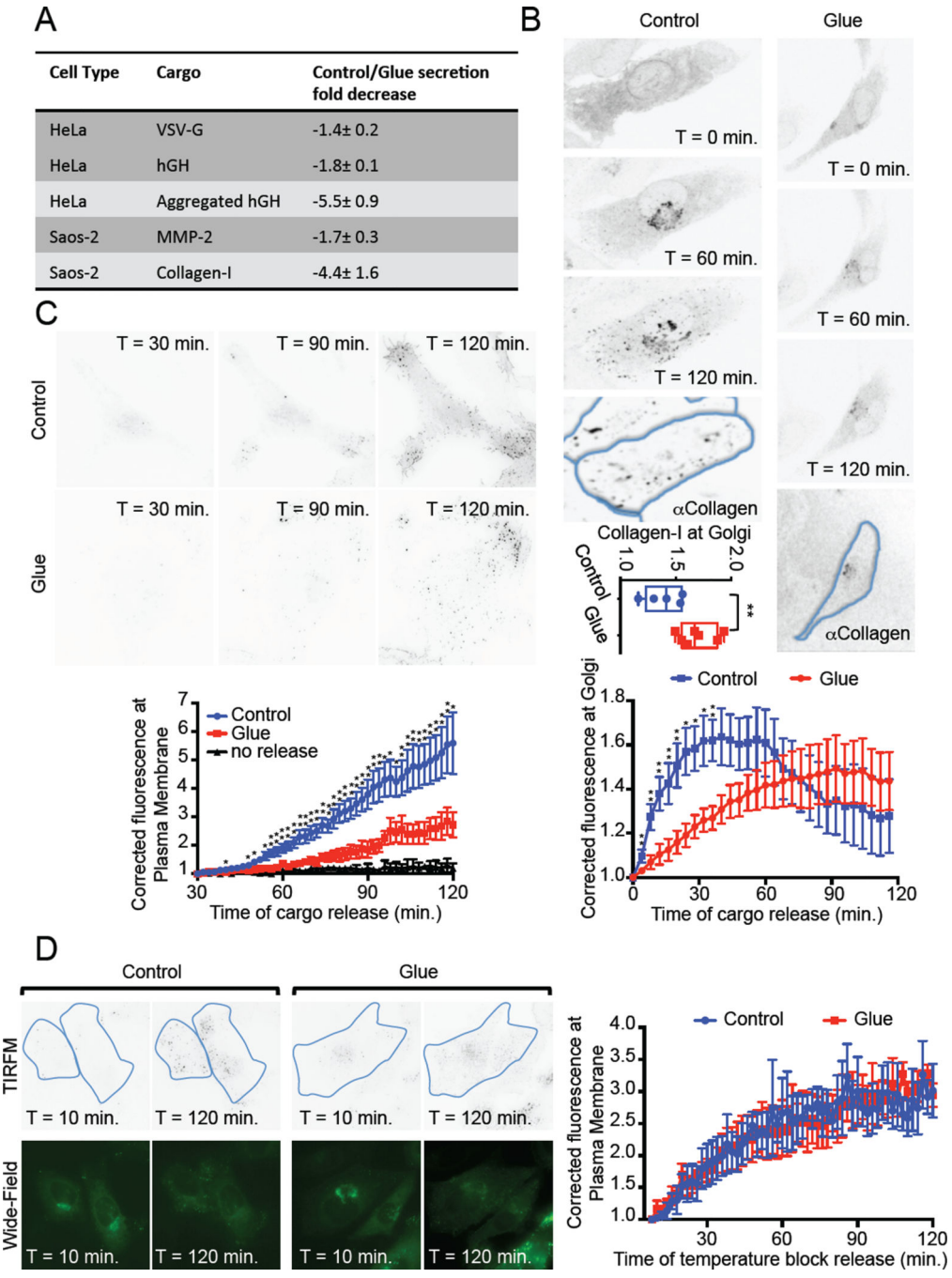

Figure 2. Cargo transport through glued Golgi

A. Table summarizing bulk transport experiments results performed on different cargoes and different cell lines (see Fig. S2 and S3). B. Saos-2 cells expressing DsRed-FRB-Golgin97, Grasp55-FKBP, Grasp65-FRB and the model cargo ssGFP-FM_4-CD8 (disaggregated form), treated (Glue) or not (Control) with Dimerizer for 16 hours, were subjected to live confocal imaging. Cargo was released by addition of Solubilizer at time 0 min. Fluorescence intensity at the Golgi was monitored, and the average of at least 5 cells taken from 4 independent experiments was plotted. After the 2 hours of live imaging, cells were fixed and immuno-

labeled for Collagen-I. The ratio of fluorescence intensity in the Golgi region over the intensity in the whole cell was plotted for each cell analyzed. C. Cells as in B were subjected to TIRF microscopy starting 30 minutes after cargo release (Solubilizer addition). Fluorescence intensity at the plasma membrane was monitored, averaged from at least 5 cells taken from 4 independent experiments and plotted. D. Cells as in C were subjected to a temperature block at 20°C for the first 4 hours of cargo release. Cells were then brought back to 37°C for 5 minutes prior to TIRF imaging as in C. Before and after live imaging, wide-field images were obtained to observe the fluorescence intensity of the cargo in the Golgi. Data from 3 independent experiments (4 cells) was averaged and plotted. *: $p<0.1$; **: $p<0.05$.

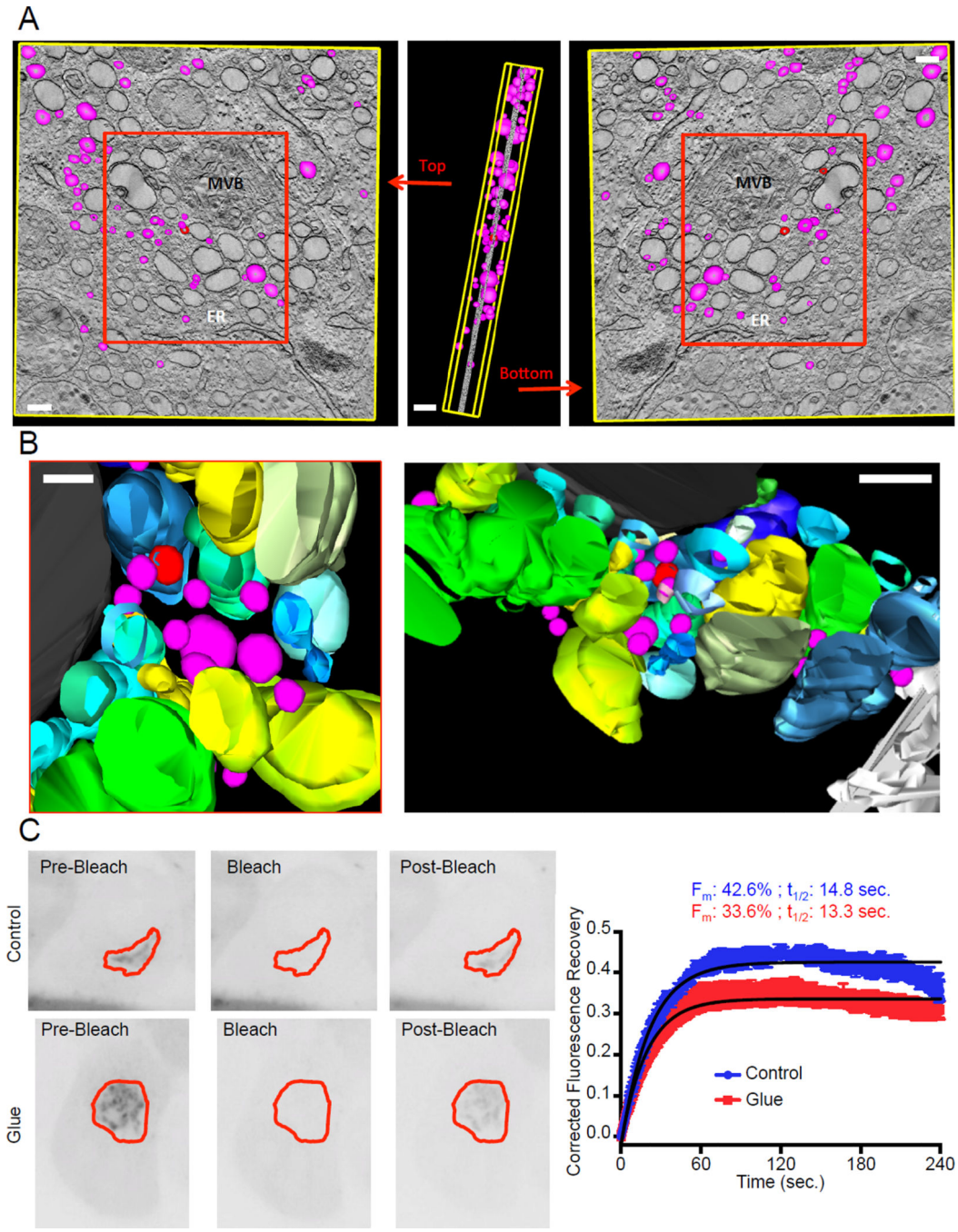

Figure 3. Vesicles form in glued Golgi

A–B. Electron tomography was performed on HeLa cells expressing DsRed-FRB-Golgin97, Grasp55-FKBP$_3$-CFP and Grasp65-FRB-YFP, treated with Dimerizer for 16 hours. 3 dimensions reconstruction was performed on 81 tilt series using the IMOD software. Golgi cisternae are represented in shades of blue, green and yellow. The colors were used to facilitate the distinction between each reconstituted partly swollen cistern. Vesicles and vesicle buds (modeled as spheres of 50 to 150 nm in diameter entirely enclosed in the thickness of the section) are magenta and red respectively. A multi-vesicular body is colored

black and the endoplasmic reticulum (ER) is white. For clarity purposes, only vesicles were modeled in A, while all the structures shown in the red box were modeled in B. Scale bars: 150 nm. C. Fluorescence Recovery After Photobleaching experiments were performed on HeLa cells expressing DsRed-FRB-Golgin97, Grasp55-FKBP, Grasp65-FRB and Arf1-GFP. GFP fluorescence was bleached and its recovery monitored in the Golgi region. Data was single-corrected and averaged over at least 5 cells taken from two independent experiments. Data was fitted on a one-phase association curve (black line).